Supporting Information

Electronic and Energy Levels Engineering of Directly Fused Porphyrin Conjugated Polymers — Impact of the Central Metal Cation

Drialys Cardenas-Morcoso[†], Eloa Vey[†], Max Heiderscheid[†], Gilles Frache[†], Nicolas Boscher[†]**

[†]Materials Research and Technology Department, Luxembourg Institute of Science and Technology, Esch-sur-Alzette, Luxembourg

**Email:* drialys.cardenas@list.lu

**Email:* nicolas.boscher@list.lu

Table of content

Scheme S1. Representation of the oCVD reactor used for the preparation of the porphyrin-based thin films from the gas-phase. **3**

Figure S1. Cyclic voltammetry of the metalloporphyrin monomers. **4**

Figure S2. Thermogravimetric analysis of the metalloporphyrin monomers. **5**

Table S1. Deposition conditions for the oCVD reaction of the porphyrins. **5**

Figure S3. Representative scanning electron microscopy of films from ZnDPP and PtDPP. **6**

Figure S4. UV-Vis-NIR absorption spectra of the oCVD fused metalloporphyrin films and the corresponding sublimed references. **7**

Figure S5. Digital pictures of the oCVD thin films before and after rinsing with dichloromethane (DCM). **8**

Figure S6. UV-Vis-NIR absorption spectra of the DCM-soluble fraction of the sublimed reference and films. **9-10**

Figure S7. LDI-HRMS spectra of the reference (sublimed) and oCVD coatings. **11-13**

Figure S8. XPS analysis of the Co 2p and N 1s core level spectra for the oCVD and sublimed reference thin films prepared from CoDPP. **14**

Figure S9. XPS analysis of the metal core level spectra for the oCVD and reference (sublimed) thin films prepared from CuDPP, NiDPP, PtDPP, PdDPP, AgDPP and RuDPP. **15**

Figure S10. LDI-HRMS simulated isotopic patterns for non-chlorinated dimers and the experimental spectrum of **pZnDPP** and **pMgDPP** coatings. **16**

Figure S11. XPS analysis of the metal core level spectra for the **pZnDPP** and **pMgDPP** coatings. **16**

Table S2. Elemental composition from XPS analysis of the reference (sublimed) and oCVD coatings. **17**

Figure S12. XPS analysis of the N 1s core level of reference (sublimed) and oCVD coatings from H_2DPP. **18**

Figure S13. XPS analysis on the valence band region of the references (sublimed) and oCVD coatings. **19**

Figure S14 Valence band minimum energy (VBM) determination in the valence band region of the XPS spectra of the reference (sublimed) (black line) and oCVD (red lines) coatings **20**

Table S3. Valence band minimum energy (VBM) determined by XPS analysis in the valence band region of the porphyrin-based thin films **21**

Figure S15. Tauc's plot from the UV-Vis-NIR absorbance measurements of the oCVD coatings, and the estimated energy band gap value. **22**

Table S4. Film thickness determined by spectroscopic ellipsometry, band gap energy (E_g) and theoretical maximum photocurrent (J_{abs}) calculated from the absorbance spectra of the oCVD processed films. **23**

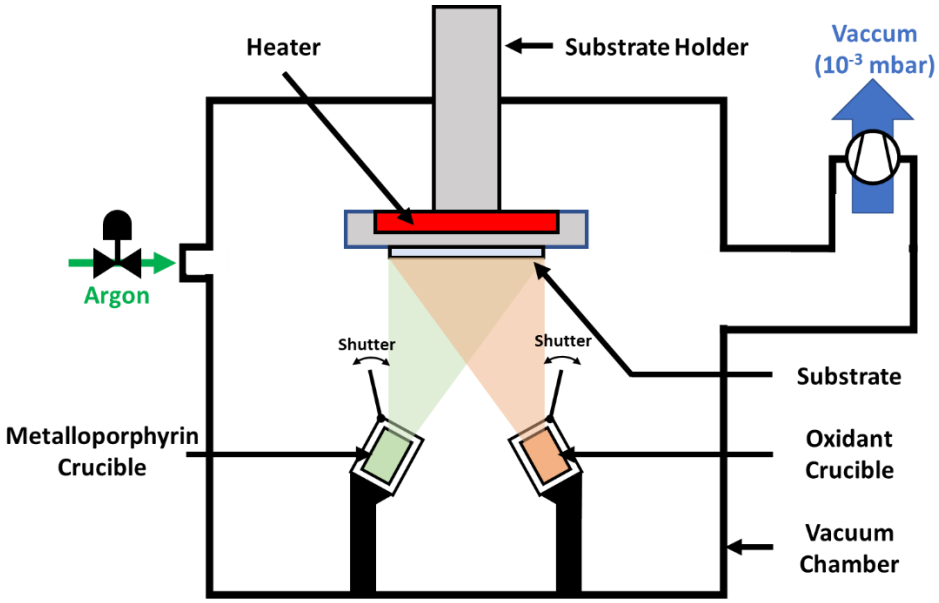

Scheme S1. Representation of the oCVD reactor used for the preparation of the porphyrin-based thin films from the gas-phase.

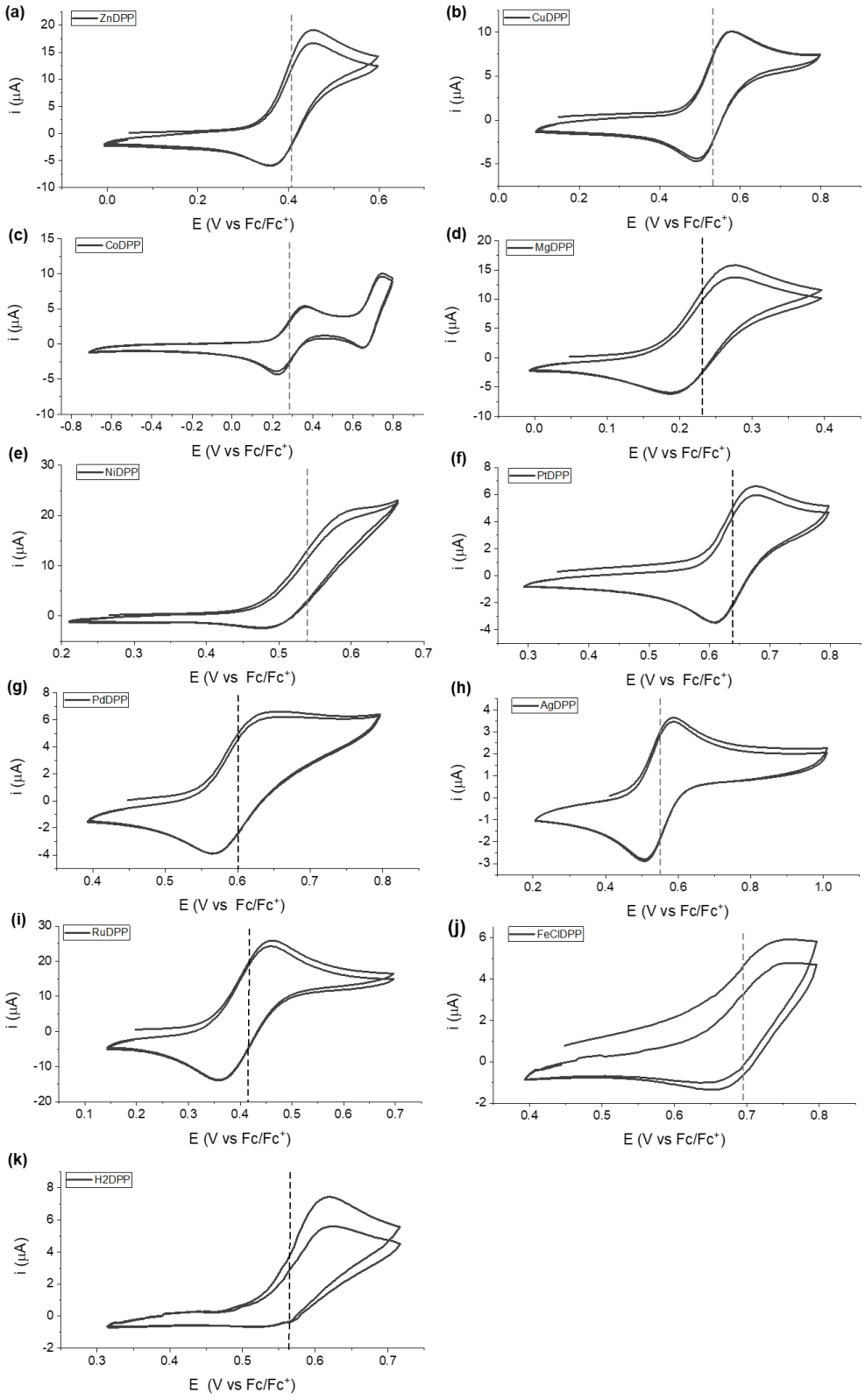

Figure S1. Cyclic voltammetry measurements to estimate the redox potential of the metalloporphyrin monomers: **(a)** ZnDPP, **(b)** CuDPP, **(c)** CoDPP, **(d)** MgDPP, **(e)** NiDPP, **(f)** PtDPP, **(g)** PdDPP, **(h)** AgDPP, **(i)** RuDPP, **(j)** FeClDPP and **(k)** H_2DPP.

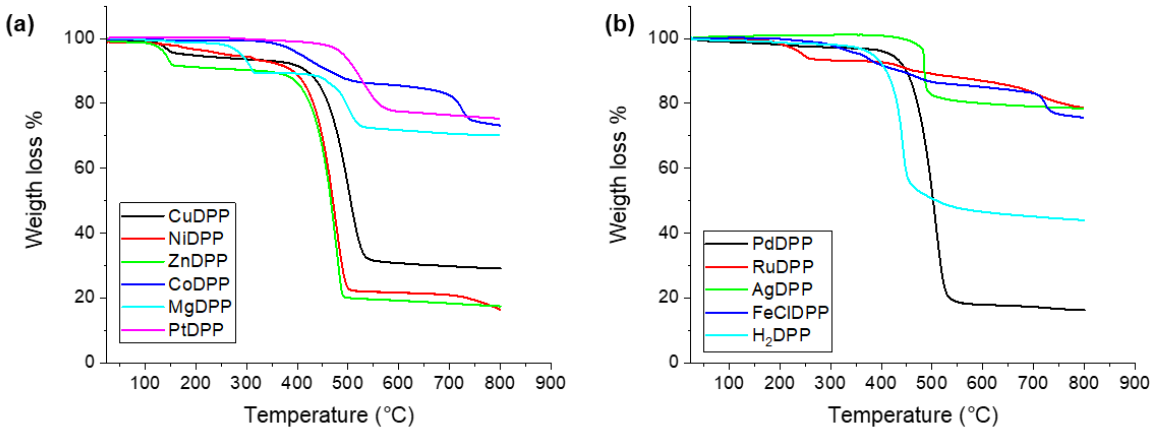

Figure S2. Thermogravimetric analysis of the porphyrin monomers used in the oCVD reaction to form fused metalloporphyrin films.

Table S1. Deposition conditions for the oCVD reaction of the porphyrins.

Porphyrin	T (porphyrin crucible) (°C)	Amount of porphyrin consumed (mg)	Amount of oxidant consumed (mg)	Ratio oxidant/porphyrin
PdDPP	270	5.4	116.4	76
CuDPP	250	4.9	114.5	76
MgDPP	260	4.5	120.6	81
NiDPP	250	5.1	124.8	79
AgDPP	260	5.1	127.6	88
FeClDPP	260	6.3	131.2	72
ZnDPP	270	5.6	120.7	70
RuDPP	270	4.7	106.9	79
PtDPP	290	6.5	114.1	72
CoDPP	255	6.0	123.6	67
H_2DPP	230	4.9	116.2	68

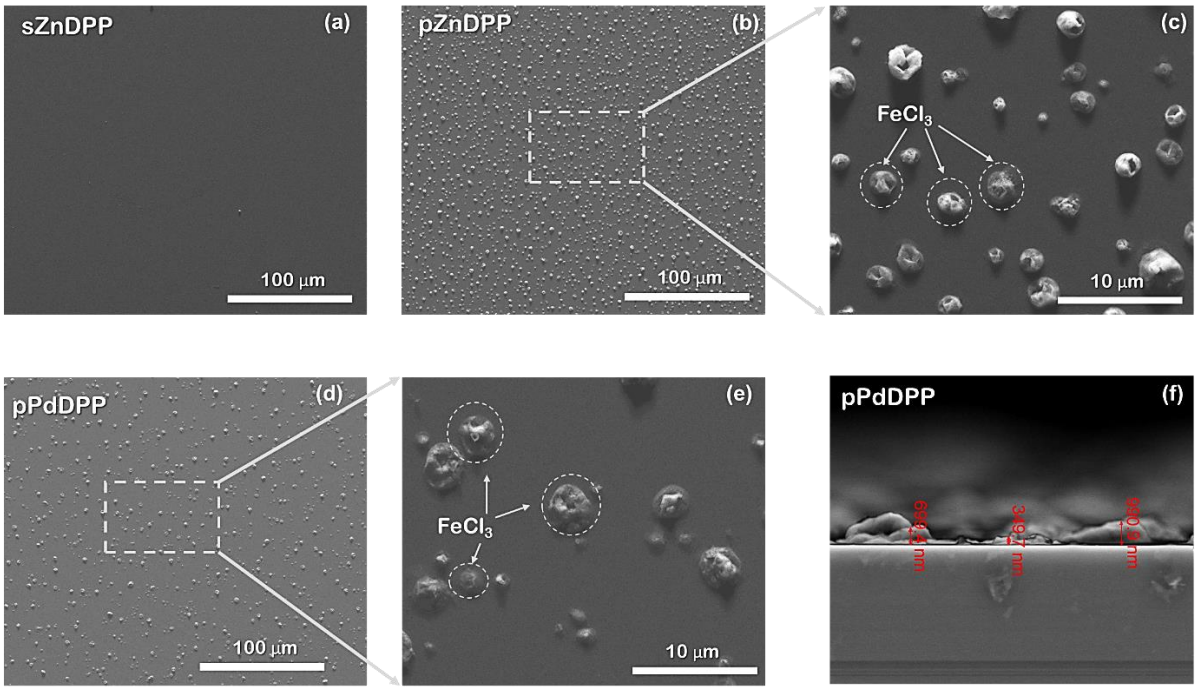

Figure S3. Representative scanning electron microscopy images of **a)** the **sZnDPP** reference (sublimed) film and **b-c)** the **pZnDPP** oCVD film (top views). scanning electron microscopy images **d-e)** top view and **f)** cross-sectional view scanning electron microscopy **pPdDPP** oCVD film.

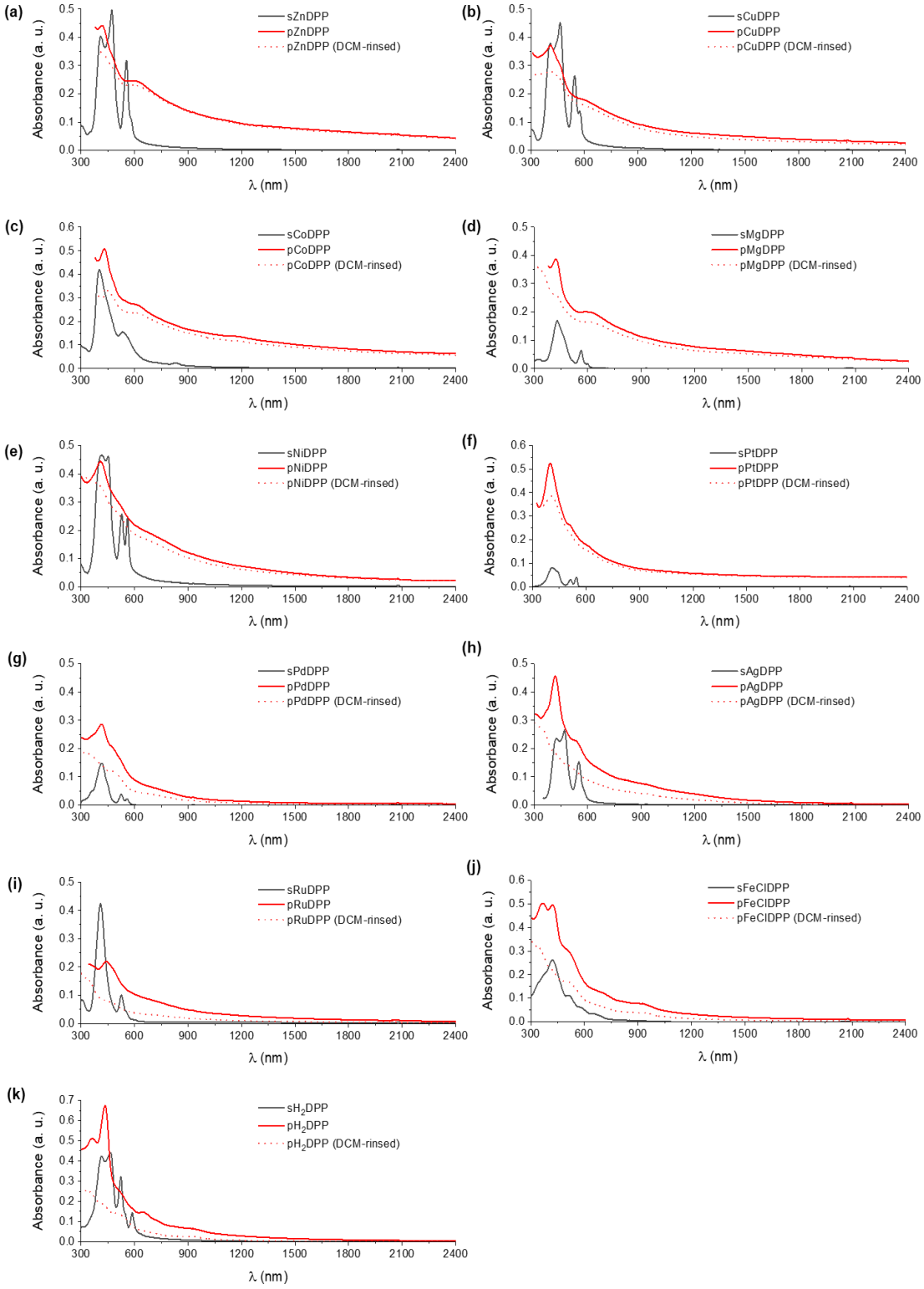

Figure S4. UV-Vis-NIR absorption spectra of the oCVD films as-deposited (red solid line) and after rinsing with dichloromethane (red dashed line). The UV-Vis-NIR absorption spectra of the reference sublimed coatings (in the absence of oxidant) are provided for comparison (black solid line).

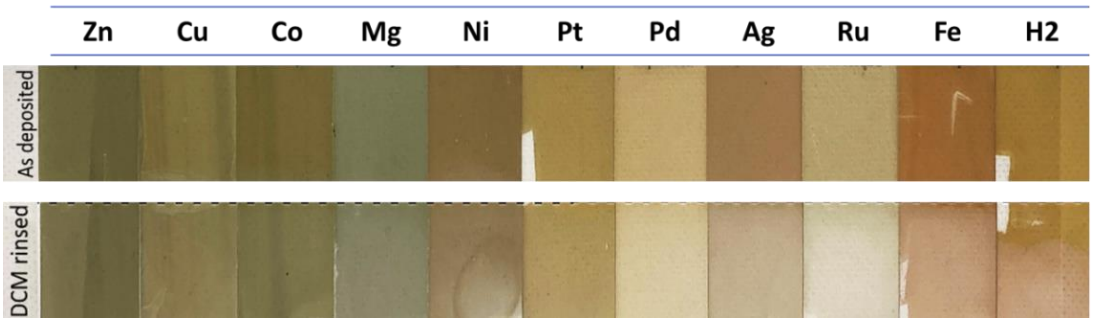

Figure S5. Digital pictures of the oCVD thin films before and after rinsing with dichloromethane (DCM).

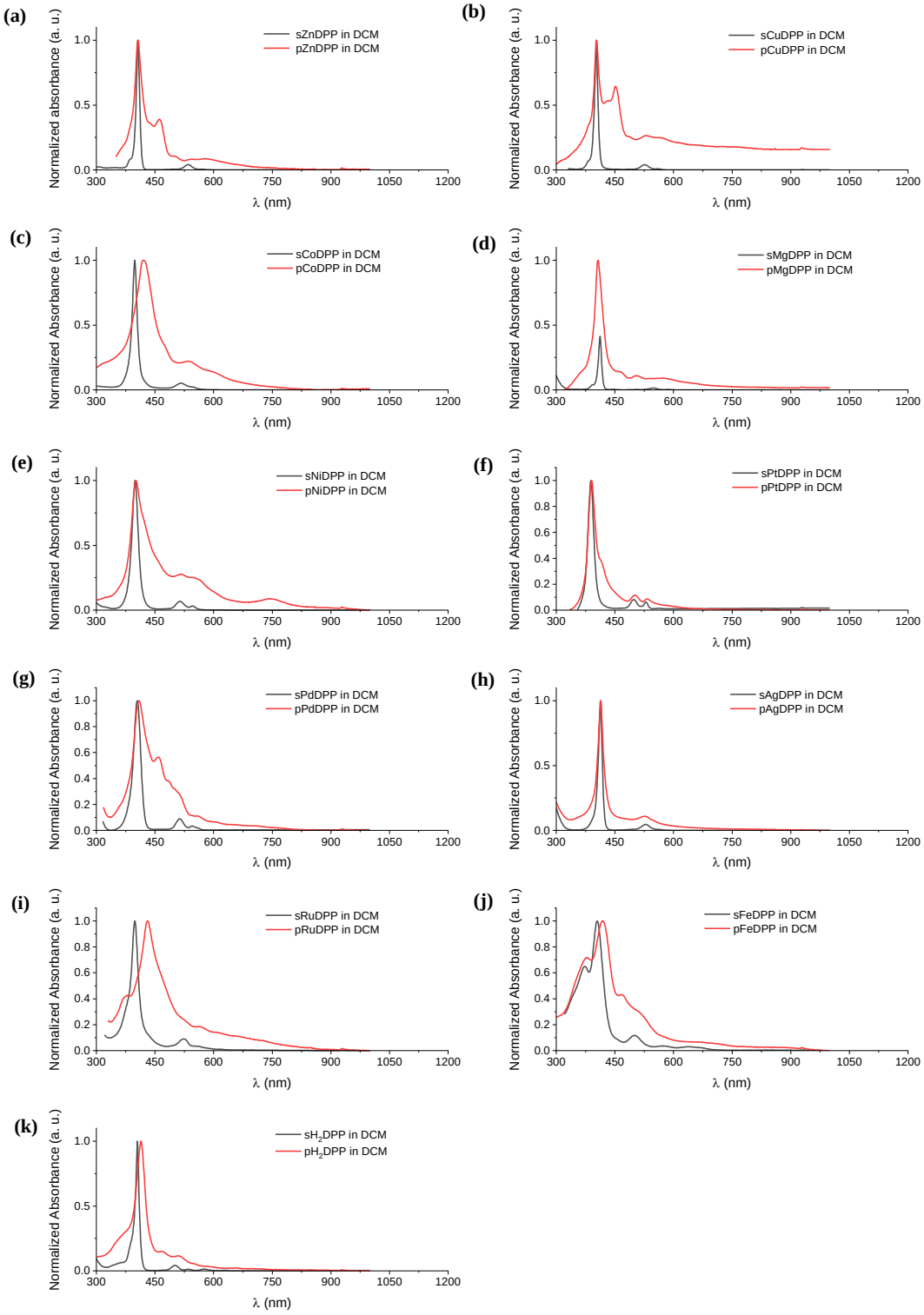

Figure S6. UV-Vis-NIR absorption spectra of the DCM-soluble fraction of the sublimed reference (black) and oCVD (red) films prepared from **(a)** ZnDPP, **(b)** CuDPP, **(c)** CoDPP, **(d)** MgDPP, **(e)** NiDPP, **(f)** PtDPP, **(g)** PdDPP, **(h)** AgDPP, **(i)** RuDPP, **(j)** FeClDPP and **(k)** H_2DPP. The Soret and Q-bands of the DCM-soluble fraction of the oCVD films exhibit a red-

shift and broadening compared to the ones of their respective reference film (monomer) dissolved in dichloromethane. This observation points to the presence of small oligomers (singly fused dimers, trimers and tetramers), as well as altered porphyrin monomers (chlorination and intramolecular cyclisation) resulting from the oCVD reaction with iron (III) chloride.

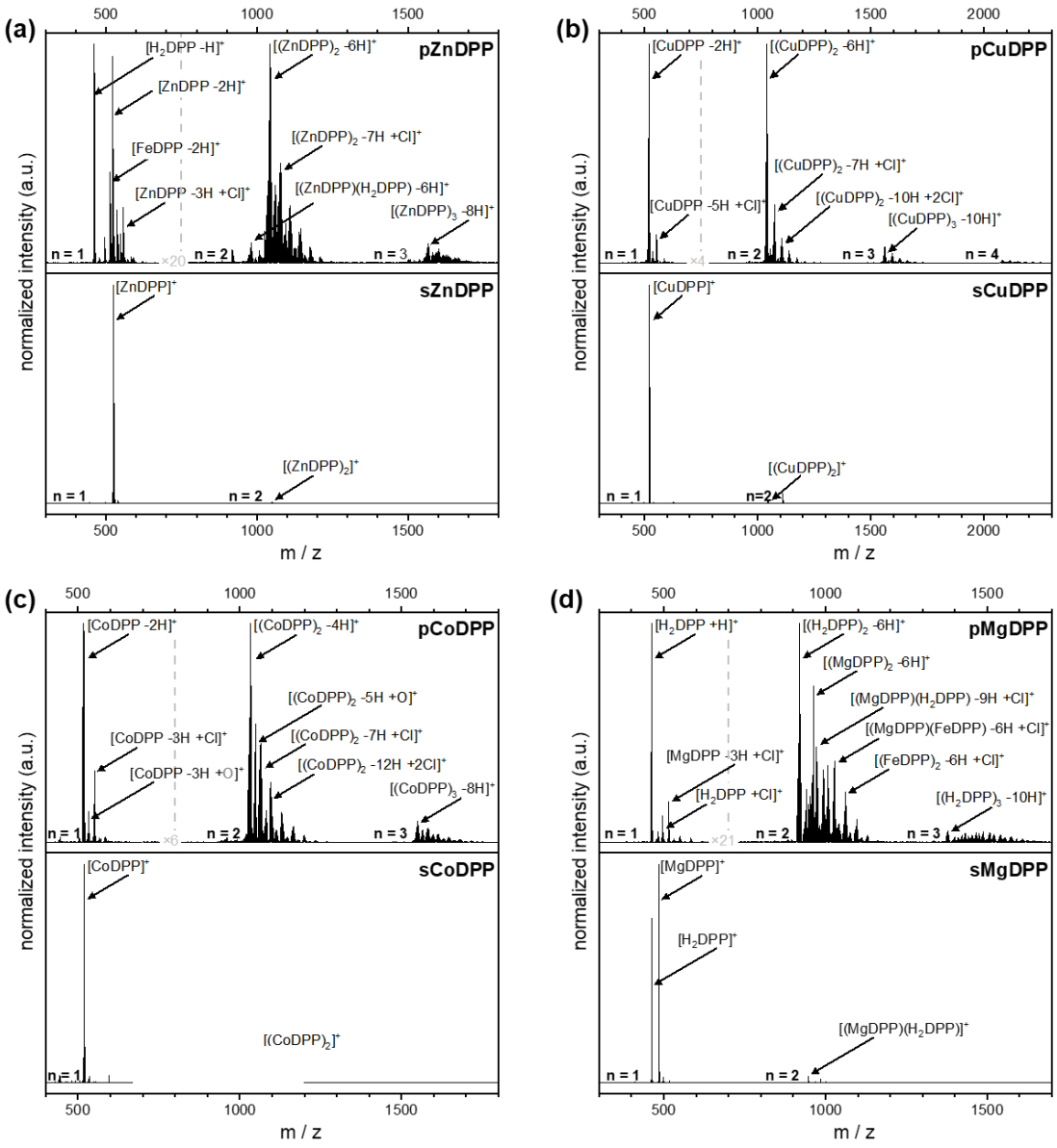

Figure S7 (a-d). LDI-HRMS spectra of the reference (sublimed) and oCVD coatings prepared from **(a)** ZnDPP, **(b)** CuDPP, **(c)** CoDPP, **(d)** MgDPP

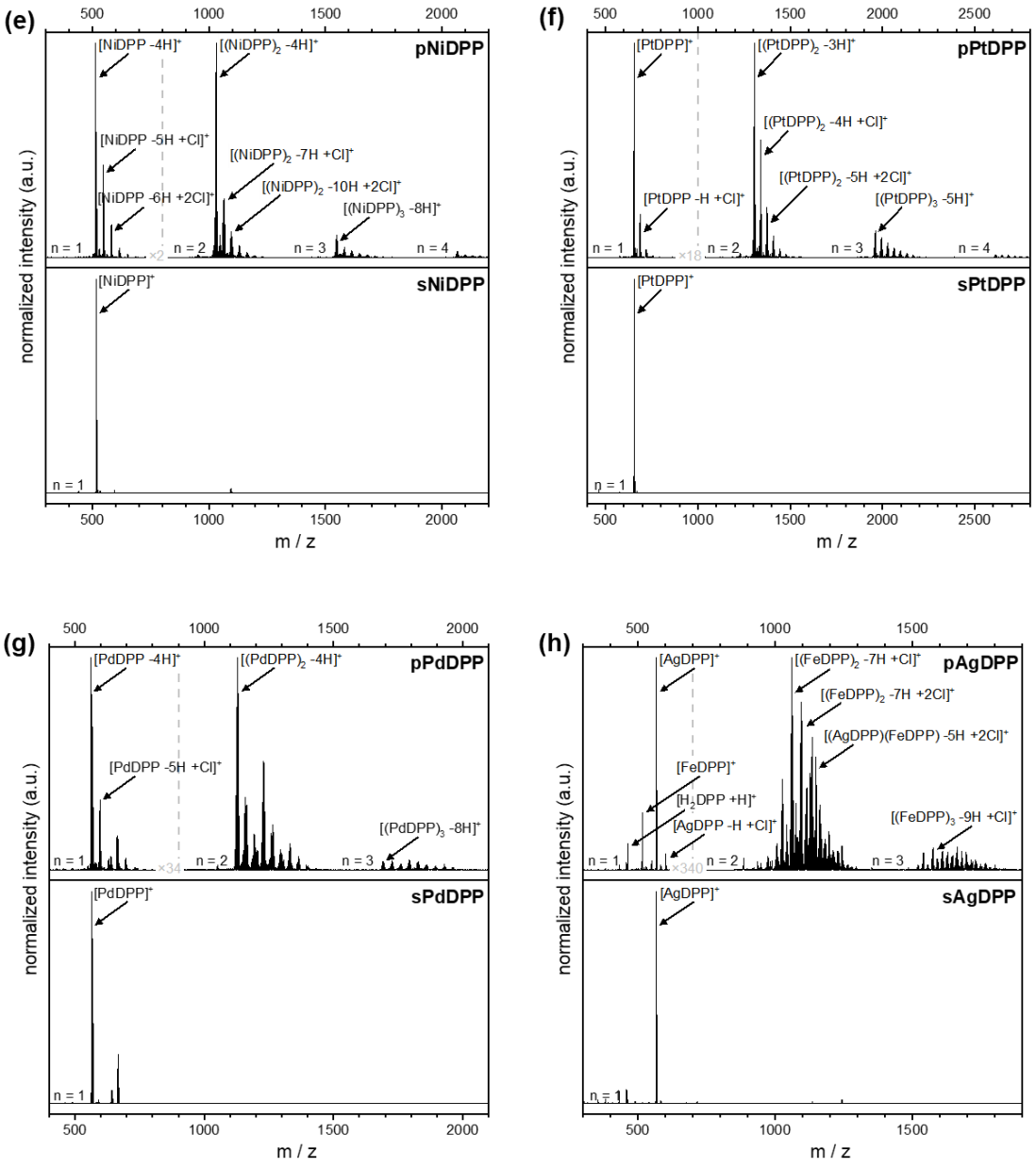

Figure S7 (e-h). LDI-HRMS spectra of the reference (sublimed) and oCVD coatings prepared from **(e)** NiDPP, **(f)** PtDPP, **(g)** PdDPP, **(h)** AgDPP

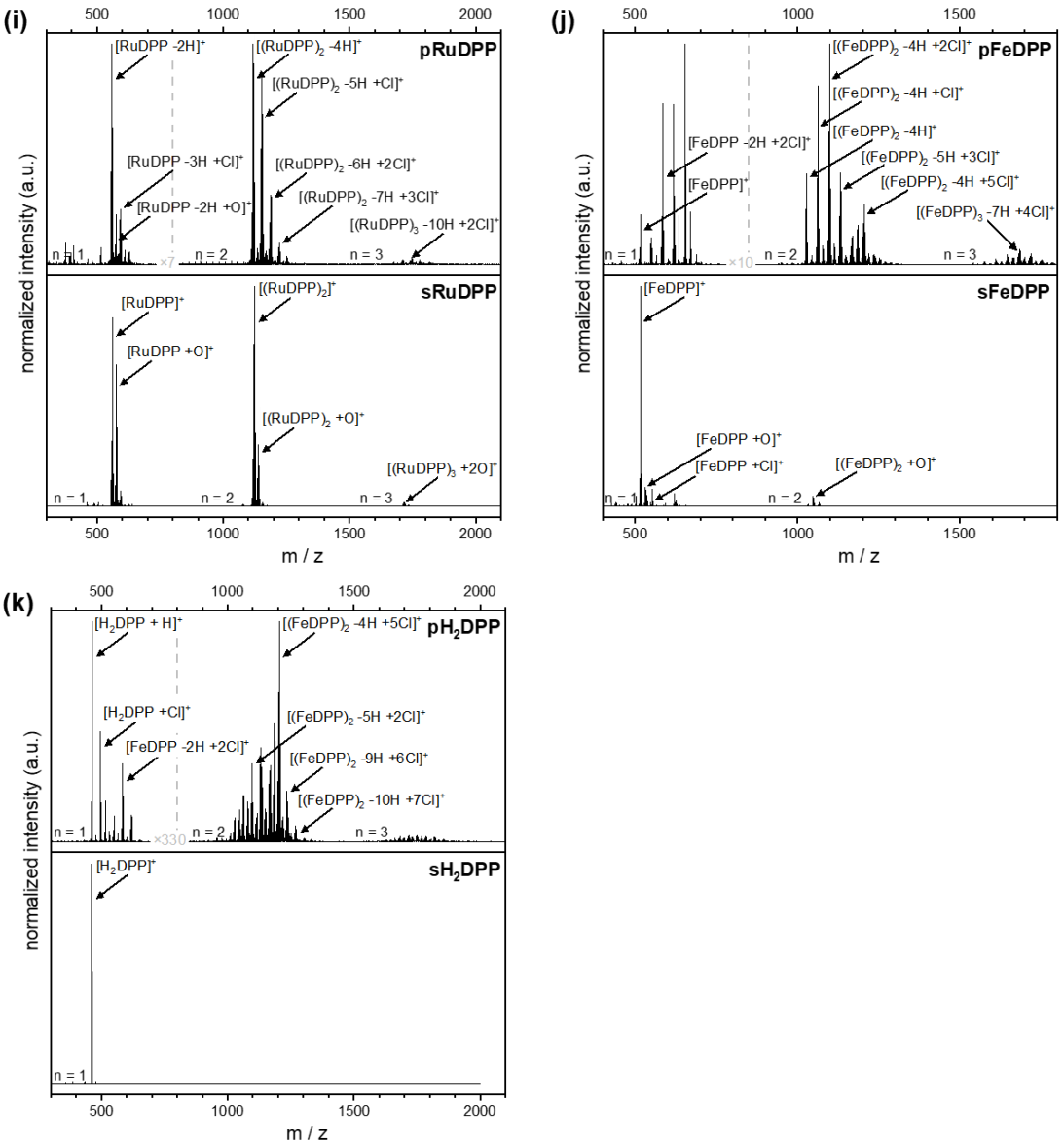

Figure S7 (i-k). LDI-HRMS spectra of the reference (sublimed) and oCVD coatings prepared from, **(i)** RuDPP, **(j)** FeClDPP and **(k)** H_2DPP.

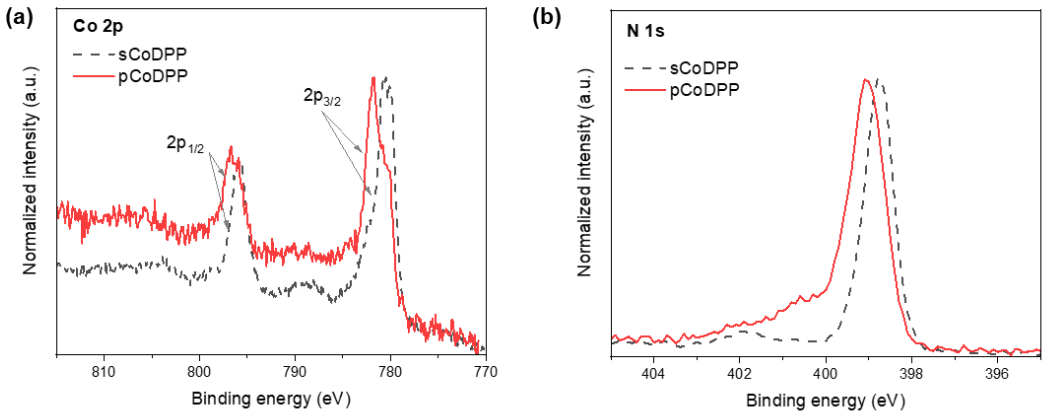

Figure S8. XPS analysis of the **a)** Co 2p and **b)** N 1s core level spectra for the oCVD (red solid line) and sublimed reference thin films (black dashed line) prepared from CoDPP. The broadness and shift towards higher binding energies of the Co 2p core level peak on the **pCoDPP** compared to the sublimed porphyrin (sCoDPP) where only Co^{2+}, indicates the presence of both Co^{2+} and Co^{3+}, as supported with the similar shift observed in the N 1s core level region.

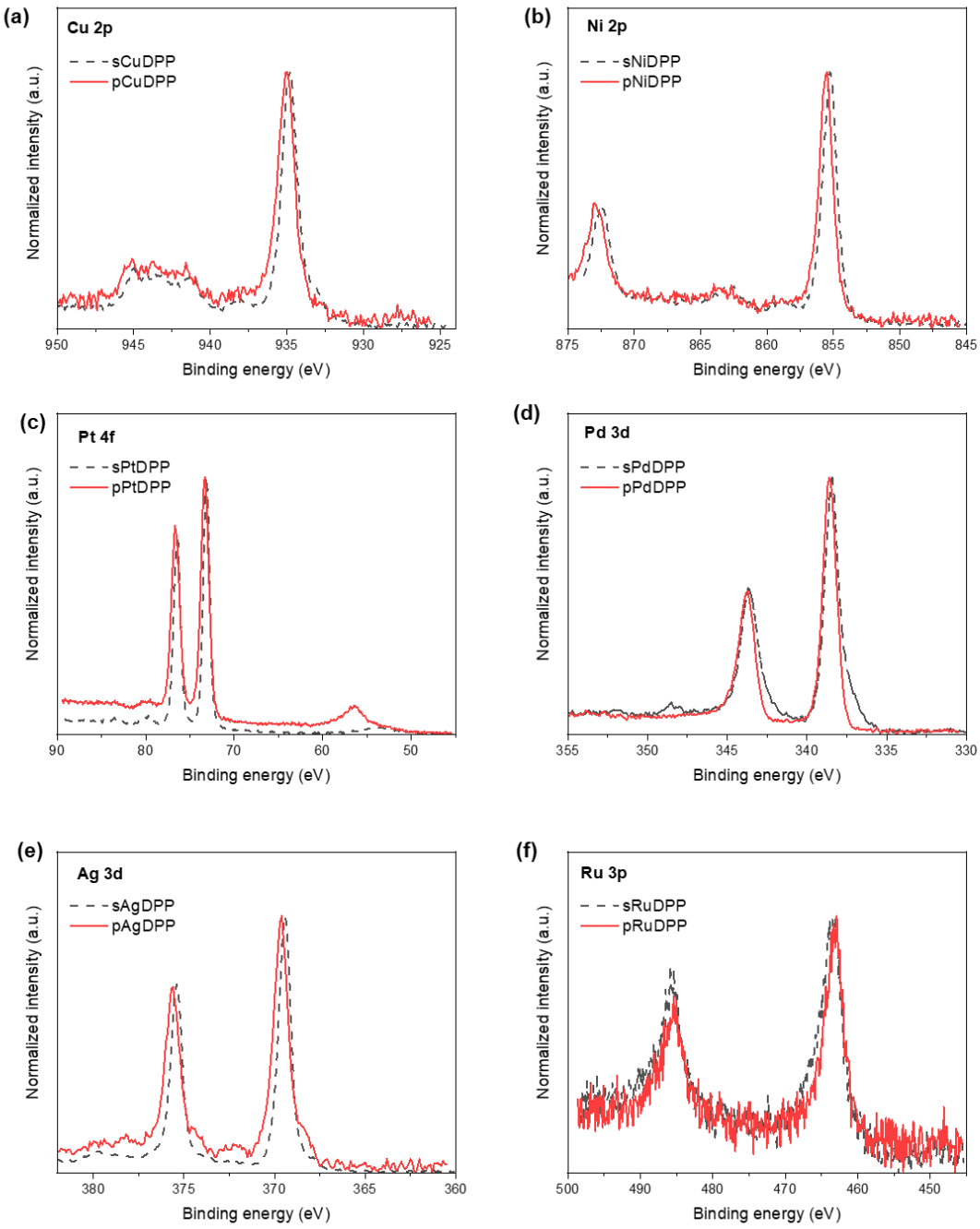

Figure S9. XPS analysis of the Cu 2p, Ni 2p, Pt 4f, Pd 3d, Ag 3d and Ru 3p core level spectra for the oCVD (red solid line) and reference (sublimed) thin films (black dashed line) prepared from **(a)** CuDPP, **(b)** NiDPP, **(c)** PtDPP, **(d)** PdDPP, **(e)** AgDPP and (**f)** RuDPP. The XPS Cu 2p, Ni 2p, Pt 4f, Pd 3d, Ag 3d and Ru 3p core level spectra remain unaltered upon oCVD reaction.

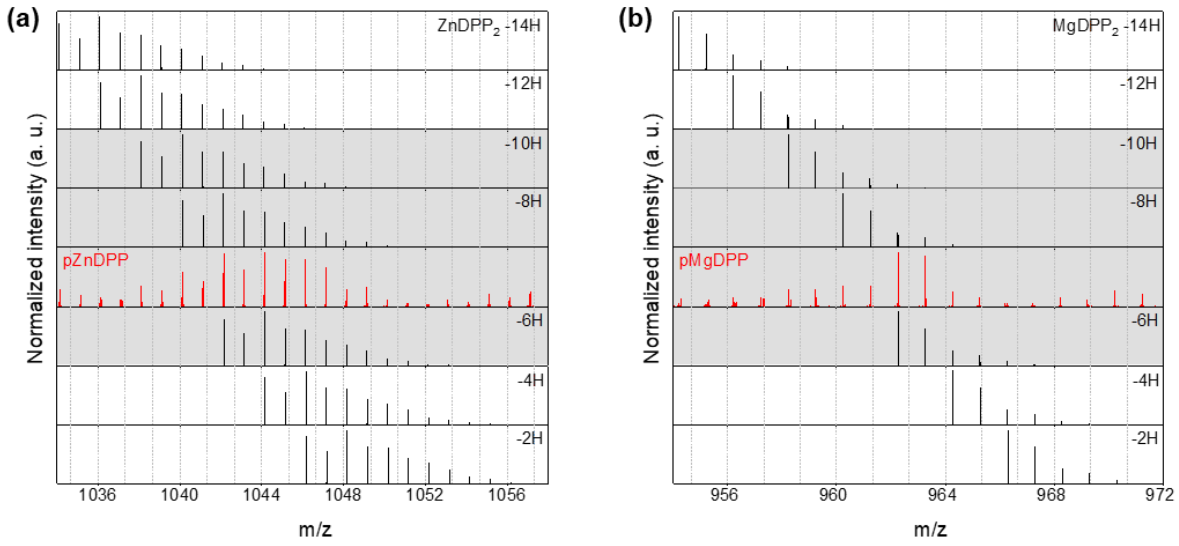

Figure S10. LDI-HRMS simulated isotopic patterns for non-chlorinated dimers **(a)** $[(ZnDPP)_2 -(H_2)_n]^+$ and **(b)** $[(MgDPP)_2 -(H_2)_n]^+$ and the experimental spectrum of **(a) pZnDPP** and **(b) pMgDPP** coatings. The comparison shows the significant contribution of peaks related to up to five C-C couplings (-10H), pointing to the formation of double and triple linkages (in accordance with the absorbance of these films in the NIR region) and intramolecular cyclisation.

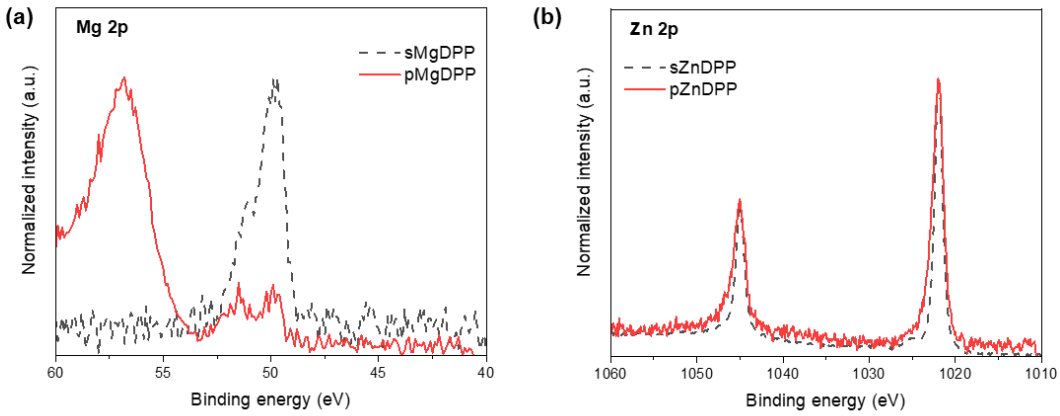

Figure S11. XPS analysis of the Mg 2p and Zn 2p core level spectra for the **pZnDPP** and **pMgDPP** coatings, respectively.

Table S2. Elemental composition from XPS analysis of the reference (sublimed) and oCVD coatings.

Sample	Cation core level	Cation %	C 1s %	Cl 2p %	Fe 2p %	N 1s %	O 1s %
sAgDPP	Ag 3d	2.7	87.3			9.9	
pAgDPP		0.9	70.4	4.7	5.6	5.0	13.4
sPdDPP	Pd 3d	2.2	88.5			9.4	
pPdDPP		1.7	79.7	2.6	2.5	7.4	6.1
sZnDPP	Zn 2p	2.3	87.7			9.9	
pZnDPP		1.0	75.0	3.9	3.9	5.4	10.9
sNiDPP	Ni 2p	2.3	88.0			9.7	
pNiDPP		1.6	80.0	2.3	3.2	6.4	6.4
sMgDPP	Mg 2p	1.7	90.5			7.6	
pMgDPP		0.9	76.8	3.5	2.9	5.8	10.1
sFeClDPP	Fe 2p/Cl 2p		87.3	1.1	3.7	7.9	
pFeClDPP			79.1	4.5	3.9	7.1	5.4
sCuDPP	Cu 2p	2.4	87.7			9.8	
pCuDPP		1.6	76.6	2.9	3.4	5.7	9.9
sCoDPP	Co 2p	3.1	87.5			9.4	
pCoDPP		1.6	79.2	3.5	2.8	6.4	6.5
sPtDPP	Pt 4f	1.9	88.6			9.5	
pPtDPP		1.5	78.1	2.3	2.9	6.7	8.6
sRuDPP	Ru 3d	2.5	89.7			7.9	
pRuDPP		1.5	69.0	5.4	5.1	4.9	14.1
sH_2DPP	(free base)	-	92.4			7.6	
pH_2DPP		-	73.4	6.3	4.7	6.8	8.7

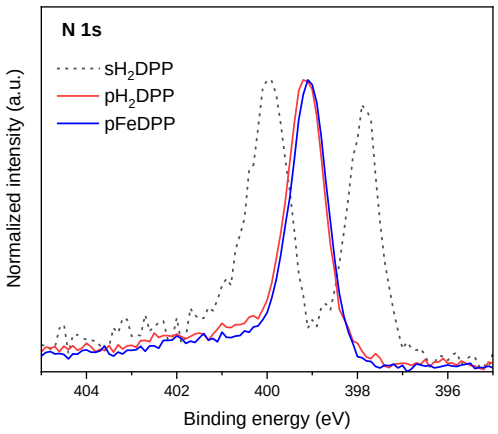

Figure S12. XPS analysis of the N 1s core level of reference (sublimed) and oCVD coatings from H_2DPP. The analysis of the **pFeDPP** coating is shown for comparison, evidencing the fully metalation of the porphyrin core.

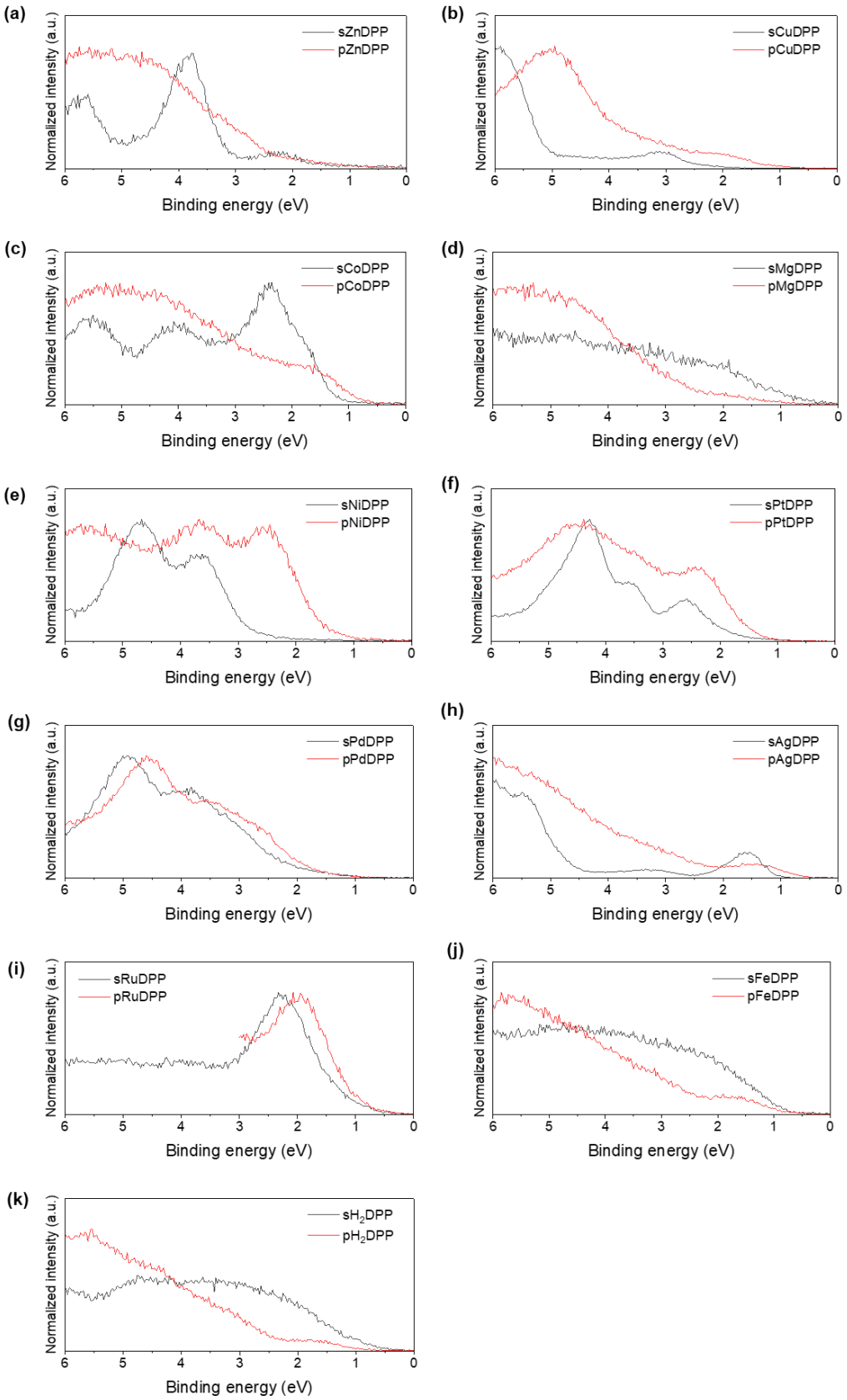

Figure S13. XPS analysis on the valence band region of the reference (sublimed) (black line) and oCVD (red lines) coatings.

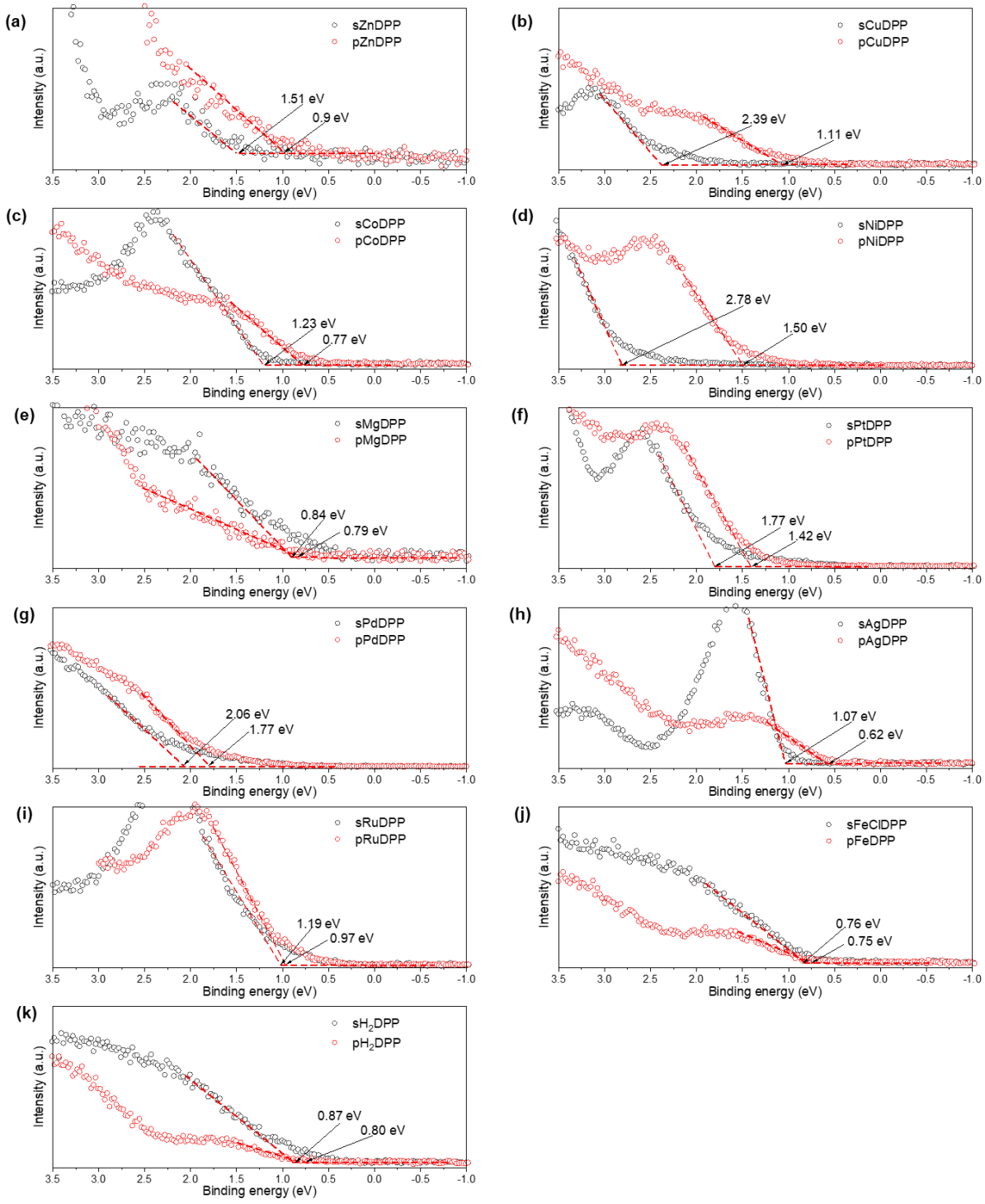

Figure S14. Valence band minimum energy (VBM) determination in the valence band region of the XPS spectra of the reference (sublimed) (black line) and oCVD (red lines) coatings.

Table S3. Valence band maximum energies (VBM) determined by XPS analysis in the valence band region of the porphyrin-based thin films.

Sample	Binding energy (eV)	Δ (eV)
sFeClDPP	0.76	0.01
pFeClDPP	0.75	
sMgDPP	0.84	0.05
pMgDPP	0.79	
sH_2DPP	0.87	0.07
pH_2DPP	0.80	
sRuDPP	1.19	0.22
pRuDPP	0.97	
sPdDPP	2.06	0.29
pPdDPP	1.77	
sPtDPP	1.77	0.35
pPtDPP	1.42	
sAgDPP	1.07	0.45
pAgDPP	0.62	
sCoDPP	1.23	0.46
pCoDPP	0.77	
sZnDPP	1.51	0.61
pZnDPP	0.90	
sCuDPP	2.39	1.28
pCuDPP	1.11	
sNiDPP	2.78	1.28
pNiDPP	1.50	

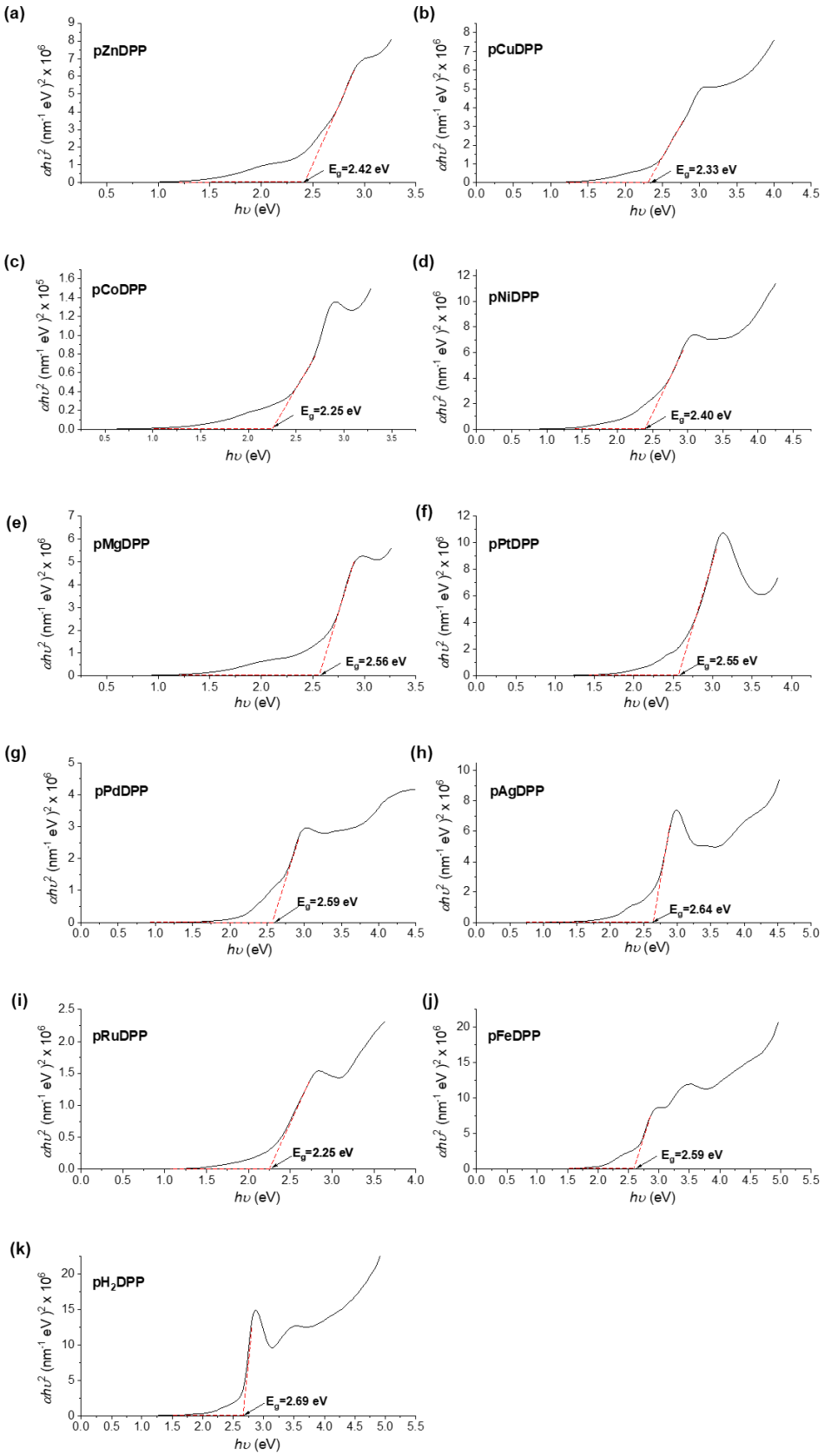

Figure S15. Tauc's plot from the UV-Vis-NIR absorbance measurements of the oCVD coatings, and the estimated energy band gap value.

Table S4. Film thickness determined by spectroscopic ellipsometry, band gap energy (E_g) estimated from Tauc's Plot, and theoretical maximum photocurrent (J_{abs}) calculated from the absorbance spectra of the oCVD processed films.

Porphyrin	Thickness (nm)	E_g (eV)	J_{abs} (mA cm^{-2})
pZnDPP	50.07 ± 0.32	2.42	5.17
pCuDPP	47.11 ± 0.30	2.33	4.05
pCoDPP	53.93 ± 0.38	2.25	5.29
pMgDPP	50.15 ± 0.15	2.56	3.00
pNiDPP	42.74 ± 0.59	2.40	4.27
pPtDPP	46.02 ± 0.15	2.55	3.40
pPdDPP	24.64 ± 0.16	2.59	2.26
pAgDPP	64.31 ± 0.97	2.64	2.73
pRuDPP	36.65 ± 0.28	2.25	3.25
pFeClDPP	52.46 ± 0.21	2.59	3.31
pH_2DPP	45.50 ± 0.47	2.69	3.01